Sky cooling-driven radiant-capacitive hydronic system for all-day building cooling

Applied Energy 406 (2026) 127260

Contents lists available at ScienceDirect

Applied Energy

journal homepage: www.elsevier.com/locate/apen

Sky cooling-driven radiant-capacitive hydronic system for all-day building cooling

Davide Forte [a], Eduardo González-Cruz [b], Lorenzo Pattelli [c], Claudio Belotti [d], Gloria Pérez [b], Pietro Asinari [a,c], Matteo Fasano [a,*]

[a] Department of Energy, Politecnico di Torino, Corso Duca degli Abruzzi 24, Torino, 10129, Italy
[b] Eduardo Torroja Institute for Construction Science (IETCC), Spanish National Research Council (CSIC), Serrano Galvache 4, Madrid, 28033, Spain
[c] Istituto Nazionale di Ricerca Metrologica, Strada delle Cacce 91, Torino, 10135, Italy
[d] Istituto Nazionale di Ottica (CNR-INO), Via Madonna del Piano 10, Sesto Fiorentino, Firenze, 50019, Italy

HIGHLIGHTS

- Validated model for a daytime radiative cooling-based hydronic system for buildings.
- DRC materials extend the cooling window by up to 3 hours over nighttime IR emitters.
- The DRC-hydronic system ensures comfort levels ~99 % throughout the cooling season.
- Such cooling systems achieve seasonal EER up to 35x that of conventional AC.

GRAPHICAL ABSTRACT

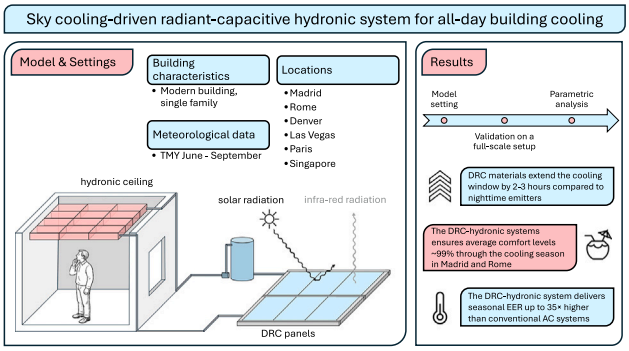

ARTICLE INFO

Keywords:
Radiative cooling
Hydronic cooling
Building
Sustainability
Heat and mass transfer

ABSTRACT

Daytime Radiative Cooling (DRC) surfaces enable heat rejection by emitting infrared radiation to the sky while reflecting solar radiation, allowing for sub-ambient cooling even under direct sunlight. This study develops and validates a transient numerical model of a DRC-based hydronic cooling system designed for building applications. The system integrates ceiling-mounted radiant capacitive modules (RCMs) with outdoor sky radiators (SRs) that dissipate indoor heat to outer space, cooling down a heat transfer fluid. The model is validated using experimental data from a full-scale demonstrator using a commercially available DRC emitter and is employed to assess system performance for a single-family building during a typical cooling season in the cities of Madrid and Rome. Compared to a system limited to nighttime radiative cooling, the DRC-enhanced setup delivers seasonal energy performance improvements of +6.2 % with a commercial DRC material and +10.3 % with an ideal broadband emitter. The study further investigates the effects of varying the surface area ratio between SRs and RCMs and alternative SR placements (rooftop vs. external surface). A fully passive building model with a DRC roof is also considered for comparison. Results show that the DRC-hydronic system can consistently maintain indoor thermal comfort throughout the cooling season, achieving seasonal energy efficiency ratios (SEER) up to 35 times higher than those of conventional air conditioning systems for the case studies analyzed, although the two systems differ in controllability and application scenarios. These findings highlight the strong potential of DRC-integrated hydronic cooling as a highly energy-efficient and sustainable alternative for the climate control of residential buildings.

* Corresponding author.
Email address: matteo.fasano@polito.it (M. Fasano).

https://doi.org/10.1016/j.apenergy.2025.127260
Received 13 October 2025; Received in revised form 3 December 2025; Accepted 12 December 2025
Available online 24 December 2025

Nomenclature

Abbreviations

AC	air conditioning
AM	air mass
BB	broadband
CC	control cell
CI	comfort index
DRC	daytime radiative cooling
DWLWAR	downwelling longwave atmospheric radiation
EC	experimental cell
HP	heat pump
HVAC	heating, ventilation & air conditioning
IOA	index of agreement
MAPE	mean absolute percentage error
RCM	radiant capacitive module
RH	relative humidity
RMSE	root mean square error
RRTM_LW	rapid radiative transfer model longwave
SEER	seasonal energy efficiency ratio
SR	sky radiator
SS	spectral selective
TMY	typical meteorological year

Subscripts and superscripts

amb	ambient
atm	atmosphere
b	building
comm	commercial
in	inlet
max	maximum
min	minimum
net	net, related to the heat transfer fluid
non-rad	non-radiative
out	outlet
p	related to the DRC panel
sol	solar
th	thermal
tot	total
w	water

Symbols

ε	emissivity (-)
θ	polar angle (rad)
λ	wavelength (m)
A	surface (m^2)
c	speed of light in vacuum ($m\ s^{-1}$)
c_p	specific heat ($J\ kg^{-1}\ K^{-1}$)
C	thermal capacity ($J\ K^{-1}$)
D	spectral downwelling longwave atmospheric irradiance ($W\ m^{-2}\ m^{-1}$)
E	energy (J)
G	solar irradiance ($W\ m^{-2}$)
h	Planck constant (J s)
h_c	convective heat transfer coefficient ($W\ m^{-2}\ K^{-1}$)
I_b	black body spectral radiance ($W\ m^{-2}\ sr^{-1}\ m^{-1}$)
k_B	Boltzmann constant ($J\ K^{-1}$)
$\dot{m}$	mass flow rate ($kg\ s^{-1}$)
q	thermal power per unit area ($W\ m^{-2}$)
Q	thermal power (W)
t	time (s)
T	temperature (K)
u	wind velocity ($m\ s^{-1}$)

1. Introduction

Air conditioning (AC) currently accounts for approximately 20 % of global electricity consumption in buildings, with demand for space cooling increasing at an average annual rate of 4 % since 2000 [1,2]. Additionally, AC is already responsible for an estimated 3.9 % of global greenhouse gas emissions, stemming from operational energy use, embodied emissions, and refrigerant leakage [3]. Enhancing building sustainability, improving the efficiency of conventional cooling systems, and developing novel, climate-friendly AC technologies are critical measures to mitigate the growing impact of space cooling on climate change [2,4–7].

Radiative cooling technologies have emerged as promising strategies to enhance building energy efficiency, either passively, via radiative cooling roofs and walls, or actively, through hydronic systems or integration with conventional AC systems [8,9]. The fundamental principle of radiative cooling involves exploiting the atmospheric transparency window (8–13 μm) to dissipate thermal energy into outer space, which acts as a renewable heat sink [10]. In recent years, Daytime Radiative Cooling (DRC) materials have been developed; these materials simultaneously emit thermal radiation in the infrared spectrum while reflecting nearly all incident solar radiation, enabling sub-ambient cooling even under high solar irradiance [11]. As a renewable cooling strategy that utilizes outer space as a heat sink, DRC offers a promising avenue for enhancing the sustainability of building envelopes and AC systems. Furthermore, DRC contributes to the mitigation of the urban heat island effect through two primary mechanisms. First, when applied to building facades and rooftops, DRC materials help lower the temperature within urban canyons [12,13]. Second, when integrated with active cooling systems, DRC enables the direct rejection of heat to outer space, rather than to the ambient environment, thereby reducing the accumulation of waste heat in urban areas.

The integration of passive DRC surfaces into building envelopes has been extensively investigated in the scientific literature [14–28]. These studies have primarily focused on quantifying the energy savings associated with the application of DRC materials, employing both experimental methodologies and building performance simulation tools such as EnergyPlus. Several works have examined the impact of DRC coatings applied exclusively to the roofs of residential, commercial, and prototype buildings [14–19], while others have extended the analysis to include both roofs and external walls of commercial and residential structures [21,24], including aesthetic appearance considerations [26,29]. Additional studies have focused on smaller-scale implementations, including full-scale prototypes, container-based units, and prefabricated buildings [22–25]. While DRC envelopes have demonstrated high performance and significant energy savings in favorable climates, in heating-dominated regions the cooling benefits during the hot season may be partially or entirely offset by the overcooling penalty in the cold season [15–17,19,21]. Additionally, standard implementation strategies for DRC coatings may be largely ineffective in most modern standard-insulated building scenarios, because the insulation limits heat transfer and reduces infrared emission from the envelope surface to the sky [15].

In active radiative cooling systems, radiative cooling materials are employed to reduce the temperature of a heat transfer fluid, typically water or air. These systems are commonly implemented using flat parallel-channel or serpentine panel configurations [30–33], although in recent years, alternative geometries based on concentrated DRC have been proposed [34]. Compared to passive radiative cooling systems, active ones offer the advantage of being controllable, allowing shutdown to prevent overcooling issues, along with the capability to store surplus cooling generated during low-demand periods, like nighttime, and release it during periods of high cooling demand. The majority of research on active radiative cooling systems has focused on their integration

with conventional building AC systems [31,32,34–39]. Among the earliest hybrid systems investigated were nighttime radiative coolers, which have been utilized either to precondition the air supplied to Heating, Ventilation, and AC (HVAC) systems, or to generate chilled water during nighttime hours to be stored and later used to enhance a heat pump (HP) operating in cooling mode [35,36]. Alternatively, DRC panels have been applied to improve the cooling capacity of the air condenser in an HP operating in cooling mode [31,37,40], or to precondition the return air entering the evaporator of an HVAC system [34]. In both scenarios, the supplementary cooling is provided via an auxiliary heat exchanger, resulting in an increase in the energy efficiency ratio of the AC system and corresponding energy savings. Additionally, during periods of low cooling demand from buildings, such as at nighttime, the surplus of DRC-cooled heat transfer fluid may be stored and subsequently utilized during peak demand periods to either supplement or replace the operation of conventional AC systems [32,38,41]. Furthermore, system configurations incorporating DRC with ground-source HPs have been proposed, with the objective of reducing the thermal load rejected into the ground [39].

Another active application of radiative cooling materials for building thermal management involves their integration with hydronic systems [42–46]. The underlying principle of these approaches is that radiative cooling surfaces can reduce the temperature of a heat transfer fluid below that of the conditioned zone, thereby enabling direct cooling through wall, ceiling, or floor-integrated heat exchanger surfaces. While the application of hydronic systems for indoor cooling is well established in the literature [47,48], their integration with radiative cooling systems remains underexplored. González et al. [42] developed an array of sky-facing panels designed to provide nighttime radiative cooling during warm seasons and solar heating during cold seasons and coupled them to the building interior via ceiling capacitive hydronic radiators. Mokhtari et al. [43] investigated the feasibility of a residential cooling system based on DRC panels in conjunction with hydronic wall and ceiling elements, while Yuan et al. [44] examined a similar configuration incorporating a hydronic floor, designed to displace a conventional residential AC system. Additional studies in this area include the development of a hydronically cooled bus station utilizing DRC panels [45], as well as an outdoor cooling structure that enhances the performance of hydronic walls through the use of visibly transparent, infrared-reflective surfaces [46].

The motivation for the present study is driven by the limited insights available on the integration aspects between DRC systems and building hydronic cooling, with the objective of achieving an efficient and nearly fully passive thermal management solution. Furthermore, to the best of the authors' knowledge, no comprehensive design analyses have been conducted to determine the optimal sizing of DRC panels coupled to hydronic heat exchangers. The present work develops and experimentally validates a numerical model for a residential building cooled by ceiling-mounted capacitive hydronic modules. These modules are supplied with chilled water produced by a field of sky-facing DRC panels. The model is employed to perform a sensitivity analysis on several design parameters of the system, including the number of operating hours, fluid flow rate, and the dimensions of both the DRC panels and hydronic modules, in two different locations: Madrid (Spain) and Rome (Italy). The results demonstrate that the proposed system can achieve high levels of thermal comfort in buildings with moderate surface-to-roof area ratios while significantly improving performance, by up to a factor of 35, compared to conventional AC systems.

2. Methods and model implementation

2.1. Plant description

The cooling system of the building analyzed and modeled in this study is schematically depicted in Fig. 1(a). It comprises four main subsystems: building, ceiling Radiant Capacitive Modules (RCMs), external Sky Radiators (SRs), and water distribution system, which includes a buffer tank, circulation pump, and piping network. Unlike conventional ceiling cooling systems, the RCMs in this configuration are *capacitive*, featuring a serpentine heat exchanger embedded in a large volume of stationary water. This stationary water mass works as the primary thermal storage, as its capacity significantly exceeds that of the buffer tank which functions as a pressure and temperature stabilizer. Locating the thermal storage within the ceiling, rather than in an externally exposed tank, enables direct thermal interaction with the building's structural masses (e.g., walls, floor, ceiling), which begin absorbing and redistributing

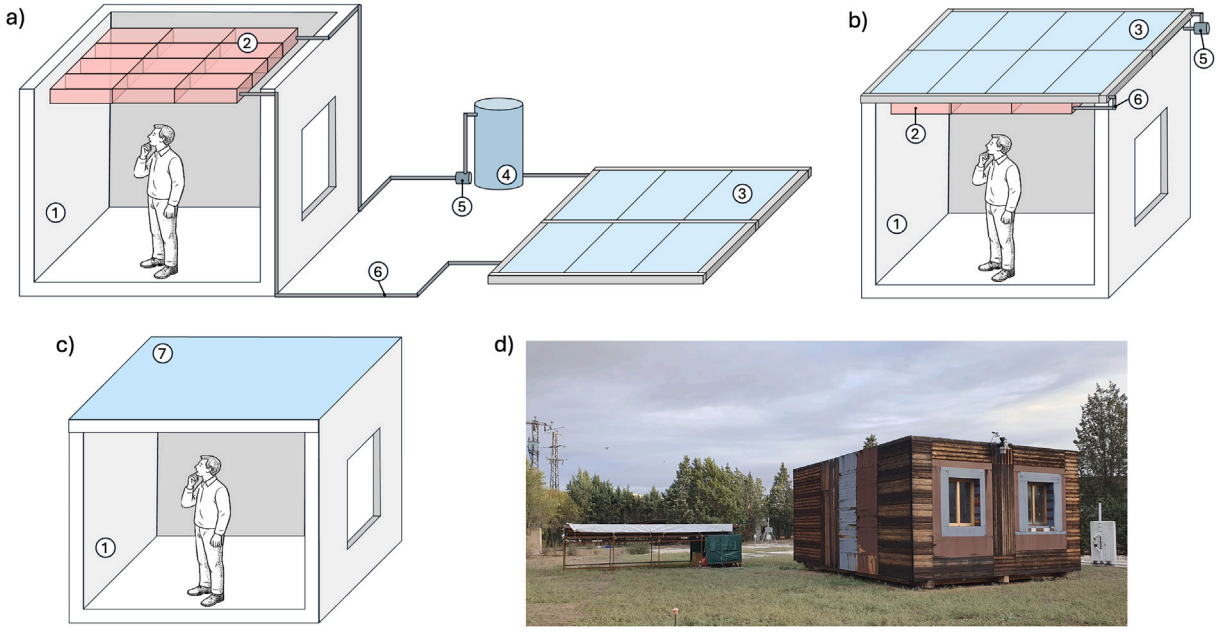

Fig. 1. Scenarios modeled. a) Hydronic cooling system with ceiling-mounted RCMs and external SRs. b) Hydronic cooling system with ceiling-mounted RCMs and rooftop SRs. c) Passive DRC material on the roof. Component legend: 1) building, 2) ceiling RCMs, 3) SRs covered with DRC material, 4) buffer tank, 5) circulation pump, 6) piping network, 7) roof covered with DRC material. Elements 4, 5 and 6 constitute the water distribution system. d) Full-scale demonstrator of a sky cooling-driven radiant-capacitive hydronic system located in Arganda del Rey (Madrid) [49].

cooling as soon as circulation starts. This configuration enhances the dynamic performance of the system, yielding a faster and more effective thermal response. A comprehensive discussion of the system design philosophy is provided in a related work [49].

Previous studies have implemented hydronic systems similar to the one analyzed here [42]. However, radiative cooling was exploited only at night, through simple high-thermal emissivity materials applied to the SRs, such as black paints. These systems aimed to cool water during the night and store it in tanks for daytime use. However, such configurations face two major limitations: (1) cooling is restricted to nighttime and (2) conventional nighttime radiative coolers absorb significant solar radiation during the day, leading to panel heating and thermal inertia effects that degrade nighttime performance. In contrast, this work employs a DRC emitter on the SRs. This approach requires materials with high emissivity in the sky window and very low solar absorptivity, as the circulating water must often be cooler than the ambient temperature to perform effective indoor cooling.

DRC materials offer a significant improvement, enabling continuous 24-hour cooling even under high solar irradiance. This concept is illustrated in Fig. 2(a)–(c), which shows the net cooling flux versus the temperature difference between the ambient (T_{amb}) and the panel (T_p) for black paint and a commercial DRC material under high, medium, and zero solar irradiance, respectively. In Fig. 2(a), the DRC material demonstrates its ability to maintain a positive net flux (i.e., the material is cooling) under 900 W m^{-2} irradiance, although the effect diminishes with increased subcooling. At night (Fig. 2(c)), both materials exhibit similar behavior due to their high emissivity. The advantage of DRC materials becomes evident under medium irradiance conditions (Fig. 2(b)), where they achieve positive net flux and moderate subcooling, unlike black paint.

Therefore, the objective of this work is to adopt DRC-coated SRs to extend the available "cooling window" from nighttime hours to periods of low-to-medium solar irradiance. This includes the early hours after sunrise and the late hours before sunset, when conventional materials fail to maintain effective cooling. This effect is further illustrated in Fig. 2(d) and (e), which show the temperature of the radiative emitter as a function of solar irradiance G. These curves are obtained by solving the steady-state thermal balance equation of the radiative cooling panels (see Eq. (1)) and validated using experimental data (see Supplementary Material, Section S5 for details). The figures demonstrate that a commercial DRC material achieves significantly lower temperatures than a black emitter under moderate and high solar irradiance.

In this work, the material referred to as *commercial DRC material* is the SpaceCool Film_Silver from SpaceCool. This material exhibits a solar reflectivity (0.25–2.5 μm) of 0.905, a broadband infrared emissivity (4–25 μm) of 0.827, and an infrared emissivity in the sky window (8–13 μm) of 0.914. Its spectral emissivity profile is shown in Fig. 2(f). The same figure also includes the emissivity profile of an ideal broadband (BB) and an ideal spectrally selective (SS) material. Further information about SpaceCool Film_Silver is available in Figure S8 and in Ref. [50].

Following the operational rationale outlined above, the hydronic cooling system functions in two distinct regimes: high irradiance and medium-to-low irradiance. During medium-to-low irradiance conditions, including nighttime, the circulation pump is activated, enabling water to flow through the hydronic network. Under this working condition, the circulating water absorbs heat from the indoor environment, resulting in a temperature increase. The warmed water exiting the RCMs is subsequently sent to the SRs, where thermal energy is dissipated to the sky. The cooled water then flows into the buffer tank before being recirculated back to the RCMs. On the other hand, under high irradiance conditions, the system is deactivated, as the SRs are unable to sufficiently subcool the water. In this regime, cooling is passively provided by the stationary cold water contained within the RCMs, which absorbs heat from the indoor space through radiative and convective mechanisms.

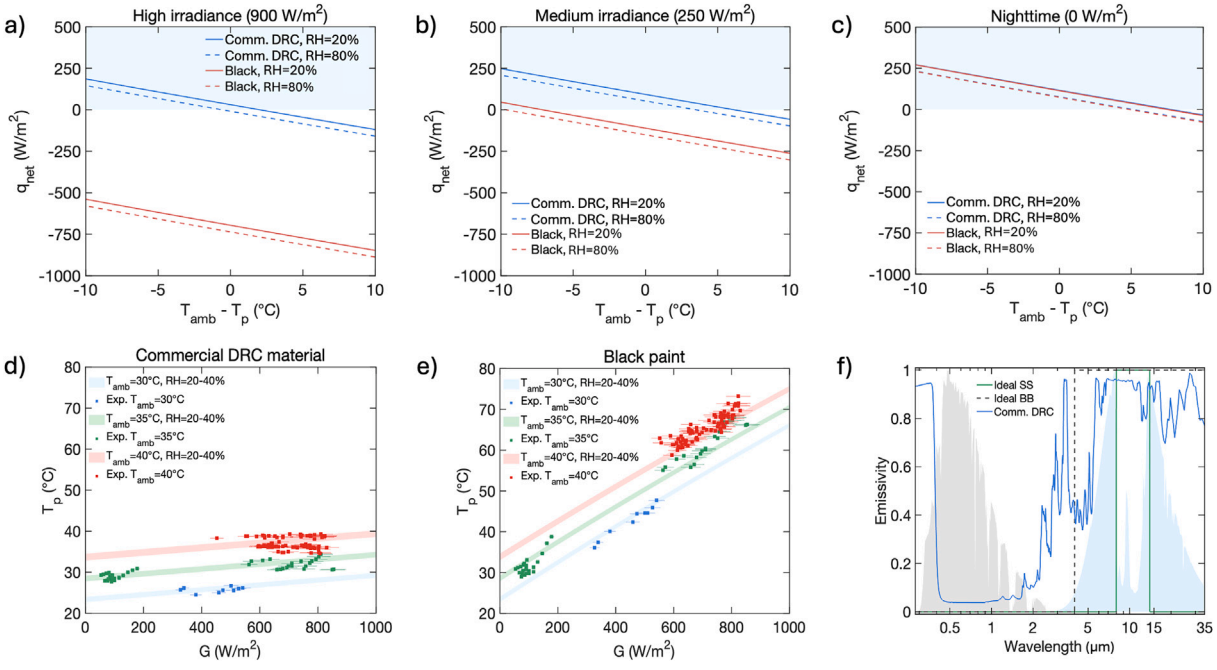

Fig. 2. Net cooling flux q_{net} (W m^{-2}) as a function of ambient-emitter temperature difference for a black paint and a commercial DRC material under conditions of: a) high solar irradiance (900 W m^{-2}), b) medium solar irradiance (250 W m^{-2}), and c) no irradiance (0 W m^{-2}). All simulations are conducted under clear-sky conditions with relative humidity (RH) values between 20 % and 80 %, and a fixed panel heat transfer coefficient of 10 W m^{-2} K^{-1}. Panels d)–e) present the steady-state emitter temperature as a function of solar irradiance for both a commercial DRC material and a black emitter, with results validated against experimental data reported in Ref. [49]. Panel f) shows the emissivity spectra of an ideal broadband emitter (dashed black), an ideal spectrally selective emitter (solid green), and a commercial DRC material (solid blue). The shaded light gray region corresponds to the normalized solar emission spectrum at A.M. 1.5 [51], while the light blue region represents the normalized atmospheric spectral radiance under clear-sky conditions at 20 °C ambient temperature and 30 % relative humidity (obtained from the model in Ref. [52]).

2.2. Model description

The hydronic cooling system and the building are implemented and modeled in the MATLAB environment. Subsystems with relatively simple physics, such as building thermal masses and the water distribution network, are modeled using Simscape, a MATLAB-based tool used to model and simulate physical systems within the Simulink environment [53]. The following subsections detail the modeling approaches adopted for each subsystem and provide information about meteorological data and locations. An overview of the structure of the model is illustrated in Figure S1.

2.2.1. Building

The modeled case study is a modern two-story single-family residential building with a habitable area of 120 m^2 and a roof area of 67.7 m^2, whose main characteristics are outlined in Tables S1-S3. Owing to the favorable roof-to-volume ratio and moderate cooling demand of the building, the roof provides adequate space to install enough SRs to meet the cooling needs. The thermal properties of the building exceed the minimum national requirements set by the regulatory frameworks of Spain and Italy, as the selected locations in this study are Madrid and Rome. All components of the building envelope and internal masses, including external and internal walls, ceiling, floor, and windows, are modeled as lumped elements. Each element is characterized by a thermal transmittance and heat capacity, determined by its stratigraphy. Comprehensive information regarding the geometry and stratigraphy of the case study building is provided in the Supplementary Material, Section S1. The data adopted in this study are sourced from authoritative publications on the European building sector [54] and national standards [55,56].

The indoor environment is modeled as a single lumped volume of moist air, characterized by its temperature (T_b) and relative humidity. The thermal model includes all major heat exchange processes: conduction through opaque and transparent surfaces, solar radiation absorbed by opaque elements and transmitted through windows, internal heat gains, and ventilation-related loads. Ventilation is modeled as a combination of infiltration and natural ventilation, with 0.3 air changes per hour (h^{-1}) from 8:00 AM to 10:00 PM, and 1 air change per hour during the remaining hours.

2.2.2. Radiant capacitive modules and water distribution circuit

The ceiling RCMs comprise galvanized steel enclosures containing approximately 50 L of stationary water. This stationary water is cooled via a copper coil through which the water previously cooled by SRs flows. A schematic of the RCMs is provided in Supplementary Material Figure S2(a). The RCMs are fully modular units connected in parallel to constitute the radiant capacitive ceiling system.

Thermal exchange between the RCMs and the building occurs through natural convection with the indoor air on the bottom and lateral surfaces, radiative heat transfer with the floor and the four surrounding vertical walls, and conductive heat transfer through the top surface, which is assumed to be in direct contact with the structural ceiling. The stationary water inside each RCM is modeled as a lumped mass characterized by a temperature T_{RCM}.

The water distribution circuit comprises a buffer tank, interconnecting pipelines, and a circulation pump. The buffer tank is a compact, thermally insulated reservoir designed to dampen pressure fluctuations in the plant. The pipelines linking the SRs, RCMs, and buffer tank are cylindrical, thermally insulated conduits made of multilayer polyethylene with raised-temperature resistance, reinforced with an intermediate aluminum layer. The circulation pump is a compact centrifugal pump operated through a simple on/off control strategy according to a predefined “cooling window”.

Given that the primary novelty of this study lies in the integration of DRC materials within the hydronic cooling system, a detailed description of the RCMs and the water distribution circuit, including geometry, modeling assumptions, and parameters, is provided in the Supplementary Material, Sections S2 and S4.

2.2.3. Sky radiators

The DRC sky radiators consist of flat-plate panels with integrated parallel channels and a nominal surface area of 2.27 m^2. Each panel comprises a polypropylene plate through which water flows within multiple parallel channels. The panel design is based on a commercial module, with a schematic shown in Supplementary Material Figure S2(b). A commercial DRC film is applied to the sky-facing surface, while the underside is insulated with a thick layer of polystyrene to minimize thermal losses. All radiators are connected in parallel, consistent with the configuration employed in prior studies [31]. Additional details concerning the panel geometry and modeling assumptions are provided in the Supplementary Material, Section S3.

The thermal behavior of a SR is governed by the following energy balance equation:

$$Q_p - Q_{sol} - Q_{atm} - Q_{non\text{-}rad} - Q_{net} = -C_p \frac{dT_p}{dt}. \tag{1}$$

Here, T_p denotes the panel temperature, and C_p (J K^{-1}) represents its total heat capacity, which accounts for the thermal mass of both the water and solid components. The term $C_p \frac{dT_p}{dt}$ corresponds to the transient thermal storage term and vanishes under steady-state conditions.

The radiative power emitted by the panel toward the sky, Q_p, is expressed as:

$$Q_p = \pi A_p \int_0^\infty \int_0^{\frac{\pi}{2}} \varepsilon_p(\lambda,\theta) I_b(\lambda, T_p) \sin(2\theta) d\theta d\lambda \tag{2}$$

where A_p is the total radiating surface area, $\varepsilon_p(\lambda,\theta)$ is the spectral-dependent and angular-dependent emissivity of the panel surface, and $I_b(\lambda, T_p)$ is the blackbody spectral radiance evaluated at the panel temperature. The blackbody spectral radiance is given by Planck’s law:

$$I_b(\lambda, T) = \frac{2\,hc^2}{\lambda^5} \frac{1}{e^{hc/(\lambda k_B T)} - 1}. \tag{3}$$

In this expression, $k_B = 1.380649 \times 10^{-23}$ J K^{-1} is the Boltzmann constant, $c = 2.99792458 \times 10^8$ m s^{-1} is the speed of light in a vacuum, and $h = 6.62607015 \times 10^{-34}$ J s is the Planck constant.

The absorbed solar radiation, Q_{sol}, is calculated as:

$$Q_{sol} = A_p G \frac{\int_0^\infty \varepsilon_p(\lambda) I_{AM1.5}(\lambda) d\lambda}{\int_0^\infty I_{AM1.5}(\lambda) d\lambda}, \tag{4}$$

where G is the total downwelling solar irradiance at the surface and $I_{AM1.5}(\lambda)$ is the solar spectral radiance at air mass 1.5, as defined in Ref. [51]. Since the panels are assumed to be installed horizontally, no angular correction for the solar angle of incidence is necessary.

The radiative power absorbed from the atmosphere, Q_{atm}, is given by:

$$Q_{atm} = A_p \int_0^\infty \varepsilon_p(\lambda) D(\lambda) d\lambda, \tag{5}$$

where $D(\lambda)$ is the spectral hemispherical downwelling longwave atmospheric radiation (DWLWAR) at the surface. $D(\lambda)$ is computed using the Longwave Rapid Radiative Transfer Model (RRTM_LW) [57,58], which requires vertical atmospheric profiles of temperature, water vapor, O_2 and trace gases including O_3, CO_2, N_2O, CO, and CH_4. The influence of cloud cover is incorporated by providing the cloud fraction profile, as well as the cloud liquid and ice water content. RRTM_LW outputs DWLWAR values integrated over the hemisphere in 16 spectral bands. Accordingly, Eq. (5) is reformulated as:

$$Q_{atm} = A_p \sum_{j=1}^{16} \bar{\varepsilon}_{p,j} \bar{D}_j \Delta\lambda_j, \tag{6}$$

where $\bar{\varepsilon}_{p,j}$ and $\bar{D}_j$ are the average emissivity and atmospheric irradiance in the j-th spectral band, respectively.

The non-radiative heat transfer, $Q_{\text{non-rad}}$, quantifies convective and conductive effects on the panel. Due to the effective bottom insulation, conductive losses through the bottom surface are neglected. Similarly, losses through the lateral surfaces are disregarded, as their area is significantly smaller than that of the sky-facing surface. Thus, non-radiative heat transfer is modeled as the wind advection heat exchange over the sky-facing surface:

$$Q_{\text{non-rad}} = A_{\text{p}} h_{\text{c,p}} (T_{\text{amb}} - T_{\text{p}}). \tag{7}$$

Here, $h_{\text{c,p}}$ is the convective heat transfer coefficient, defined as [32]:

$$h_{\text{c,p}} = 8.3 + 2.5 \frac{u}{u_0}, \tag{8}$$

where u is the wind velocity and $u_0 = 1$ m s^{-1} is a constant. Q_{net} is the heat brought by the thermal fluid to the panel, simply defined as:

$$Q_{\text{net}} = \dot{m}_{\text{w}} c_{\text{p,w}} \left(T_{\text{w-in}} - T_{\text{w-out}} \right), \tag{9}$$

where $\dot{m}_{\text{w}}$ is the water mass flow rate inside the SR, $c_{\text{p,w}}$ is the specific heat of water (J kg^{-1} K^{-1}) and $T_{\text{w-in}}$, $T_{\text{w-out}}$ are the inlet and outlet temperatures of water, respectively.

2.3. Meteorological data

The DRC-driven hydronic cooling system was evaluated during the cooling season (June to September) at two locations: Madrid (40.25°N, 3.50°W) and Rome (42.00°N, 12.50°E). The four-month period was selected based on the Typical Meteorological Year (TMY) reported in PVGIS, developed by the European Commission's Joint Research Centre [59], constructed according to ISO 15927–4 standards [60].

Following TMY selection, the corresponding hourly meteorological variables were obtained from the ERA5 reanalysis [61], specifically:

(1) ambient air temperature at 2 m, used as air temperature;
(2) dew point temperature at 2 m, used to calculate relative humidity;
(3) soil temperature at 28–100 cm depth, used as ground temperature;
(4) wind velocity at 10 m;
(5) average surface downwelling shortwave radiation flux, used as solar irradiance.

Data for the RRTM_LW model employed in DWLWAR calculations were also sourced from ERA5 and from climatology as detailed in Ref. [62].

The locations of Madrid and Rome were selected based on two main considerations. First, Spain and Italy are among the most favorable regions in Europe for radiative cooling applications [63]. Second, the two cities exhibit different climatic conditions, allowing the experimental setup to be evaluated under varying weather scenarios. According to the updated Köppen–Geiger classification [64], Rome has a hot-summer Mediterranean climate, with dry summers and mild winters (Csa climate type). Madrid, instead, is situated on the boundary between the Csa climate and the BSh climate type, the latter corresponding to a semi-arid climate with hot summers.

3. Results

3.1. Model validation

The model was first successfully validated on a full-scale demonstrator located in Arganda del Rey (40.314° N, 3.482° W), shown in Fig. 1(d), before being used for extrapolations to a large-scale residential DRC-hydronic cooling system. The demonstrator, experimental setup, and acquired data are comprehensively described in a separate publication [49]. The demonstrator consists of a small building (8.8 m × 7.0 m × 2.9 m), divided into three thermal zones: two rooms and a lobby. One room, equipped with the RCMs, is designated as the experimental cell (EC), while the other is the control cell (CC) and remains unconditioned. Externally, the system includes five parallel-connected SRs and a thermal storage unit. Additionally, smaller square samples (20 cm × 20 cm) of DRC and non-DRC materials, not connected to the hydraulic system, were installed and sensorized.

The system layout corresponds to that shown in Fig. 1(a). The model validation was conducted using two experimental series, each lasting five days: Series 1 (20/08–24/08/2024) and Series 2 (08/08–12/08/2024). In Series 1, the SRs were coated with a commercial DRC material (SpaceCool Film_Silver), while in Series 2, the panels were uncoated, exposing the black polypropylene surface to the sky, to act as a nighttime-only radiative cooling material. In both cases, the circulation pumps operated from 10:00 PM to 8:00 AM. Validation was performed over the final four days of each series (21/08–24/08/2024 for Series 1 and 09/08–12/08/2024 for Series 2), excluding the first day to smooth the errors generated from the unknown initial conditions of some of the building subsystems.

Detailed design and operational parameters for the experimental series are provided in Tab. S13. Model accuracy was assessed using mean absolute percentage error (MAPE), root mean square error (RMSE), and index of agreement (IOA), as defined in the Supplementary Material, Section S5.

Fig. 3(a) and (b) compare measured and simulated temperatures of the EC and CC for Series 1 and 2, respectively. The results demonstrate high agreement, with MAPE values of 0.67 % and 0.64 % for the CC and 0.70 % and 0.86 % for the EC. In both cases, the RMSE remains below 0.3 °C. Fig. 3(c) and (d) present the RCM temperature comparisons for Series 1 and 2, yielding MAPE values of 1.52 % and 1.49 %, respectively.

Fig. 3(e) and (f) report the surface temperatures of the passive square samples for Series 1 and 2, featuring the DRC material and black polypropylene, respectively. The MAPE values are 5.58 % and 4.19 %, with RMSE values of 1.4 °C and 2.2 °C. These results are consistent with other studies [65] and validate the DRC material model. The simulations also reproduce the expected thermal behavior: the DRC sample remains consistently below ambient temperature throughout the day, including periods of peak solar irradiance, whereas the black emitter achieves sub-ambient temperatures only during nighttime hours (approximately between 8:00 PM and 8:00 AM).

Fig. 3(g) and (h) compare simulated net fluxes of the SRs with experimentally derived values, including uncertainty. The model predictions fall within the uncertainty bounds. MAPE values are approximately 10 % for both series, even though the results are largely influenced by the discrepancies at the initial peak due to system startup. To provide a more comprehensive assessment, IOA is also considered, yielding values of 0.97 for Series 1 and 0.95 for Series 2.

Overall, the comparison between the numerical model and the experimental series provides full validation of the model and confirms the high accuracy achieved in the prediction of the transient behavior of the building, the RCMs, and the SRs. Although the lumped-mass approach already yields satisfactory performance, higher accuracy could be obtained through the inclusion of thermal stratification in the indoor air and in the stationary water inside the RCMs.

3.2. Extension of operation hours

The validated model is employed to assess the impact of a DRC-driven hydronic cooling system on a full-scale single-family building during a TMY cooling season in the Madrid climate. The analysis includes a performance comparison with an identical system using a conventional nighttime emitter coated with black paint (broadband infrared thermal emissivity of 0.9 and solar reflectivity of 0.1). Fig. 4 presents the effect of varying the number of charging (pumping) hours on the overall performance of the hydronic cooling system. Charging hours denote the number of hours per day during which water is circulated through the closed loop connecting the SRs and RCMs. The minimum number

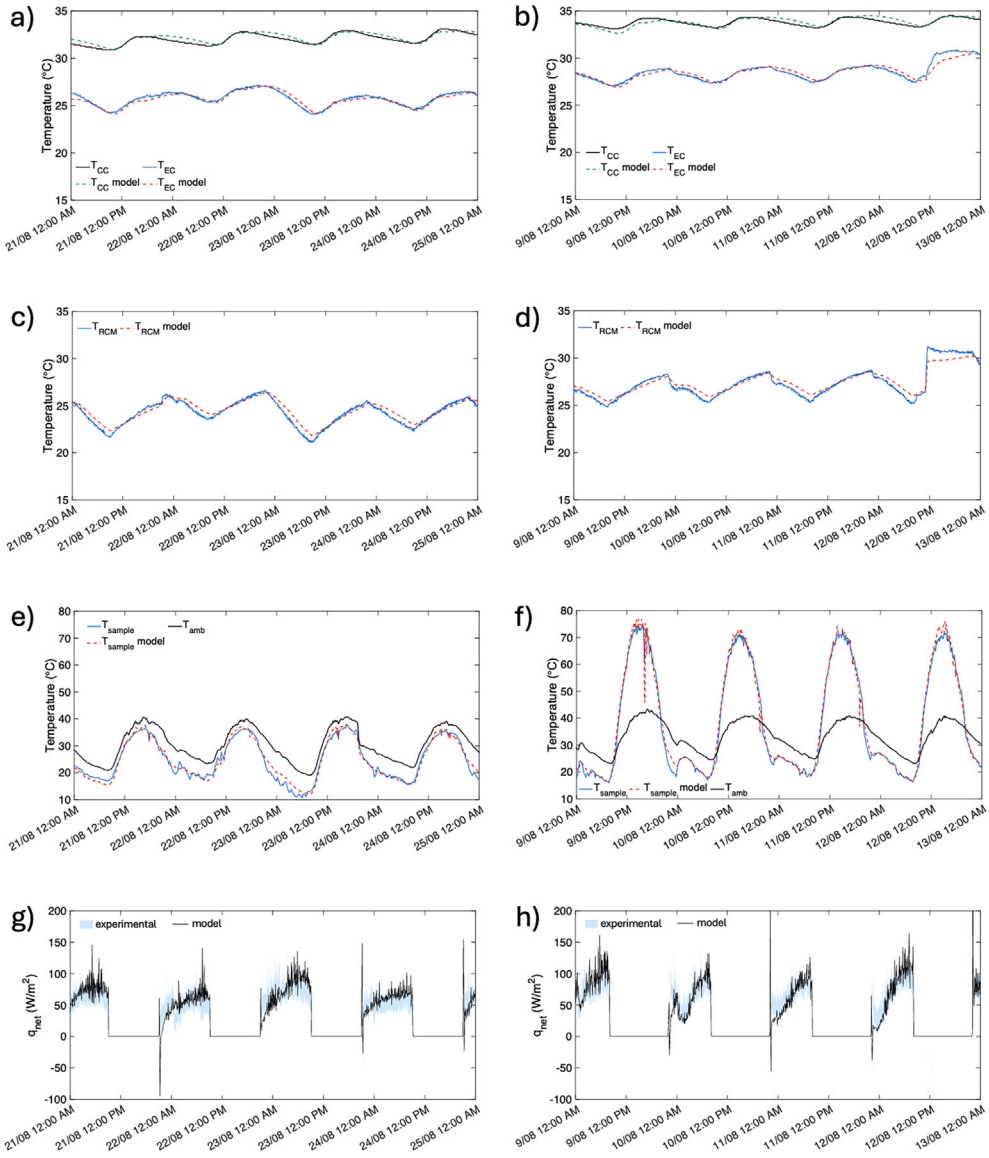

Fig. 3. Model validation against experimental results from the full-scale demonstrator in Ref. [49]. Panels a), c), e), and g) correspond to Series 1 (DRC emitter), while panels b), d), f), and h) correspond to Series 2 (black emitter). a–b) Temperature of the EC and CC. c–d) Water temperature in the RCMs. e–f) Surface temperature of the 20 cm × 20 cm material samples. g–h) Net flux of the panels.

of charging hours evaluated is 10, which includes all nighttime and low-irradiance hours in Madrid, from 10:00 PM to 8:00 AM. The pumping period is then progressively extended in 1 h-steps, expanding the time window symmetrically by 30 minutes at both ends. For instance, 11 pumping hours correspond to a window from 9:30 PM to 8:30 AM, 12 hours from 9:00 PM to 9:00 AM, and so forth. Three DRC materials are included in the test: the commercial DRC emitter, an ideal BB emitter, and an ideal SS emitter. Their emissivity profiles are shown in Fig. 2(f). These simulations are carried out for a constant number of SRs and RCMs, set respectively to 25 and 60. These values are chosen because, as will be later demonstrated in Section 3.3.2, they are able to ensure a suitable comfort level in the building and lie reasonably close to the optimal working conditions of the plant for the building located in Madrid.

Fig. 4(a) and (b) display the energy removed by the RCMs over the entire cooling season (June-September), with the system operating at flow rates of 0.25 and 1 L min^{-1} m^{-2}, respectively. These flow rates are normalized by the area of the SRs, which is essential for correctly scaling the total flow within the system according to the emitter surface area, ensuring effective water cooling in each panel. The energy removed by the RCMs is a representative figure of merit for evaluating the effectiveness of the cooling system. When using the black emitter, the system achieves its peak seasonal energy removal at 11 and 10 pumping hours for the flow rates of 0.25 and 1 L min^{-1} m^{-2}, respectively. In contrast, the use of a commercial DRC emitter results in a shift of the optimal operating window to 13 and 12 hours, enabling a two-hour extension in both cases. This expansion reflects the enhanced radiative performance of the emitter, particularly during early morning and late evening hours. Ideal BB and SS emitters demonstrate an even greater impact, allowing the optimal pumping duration to extend by three hours under both flow rate scenarios. In terms of relative performance improvement, the commercial DRC emitter increases total seasonal energy removal by +6.2 % compared to the black emitter. The ideal BB and SS materials further improve energy removal by +10.3 % and +6.3 %, respectively.

The curve corresponding to the black emitter declines as soon as the pumping period extends into daytime hours. This behavior is attributed

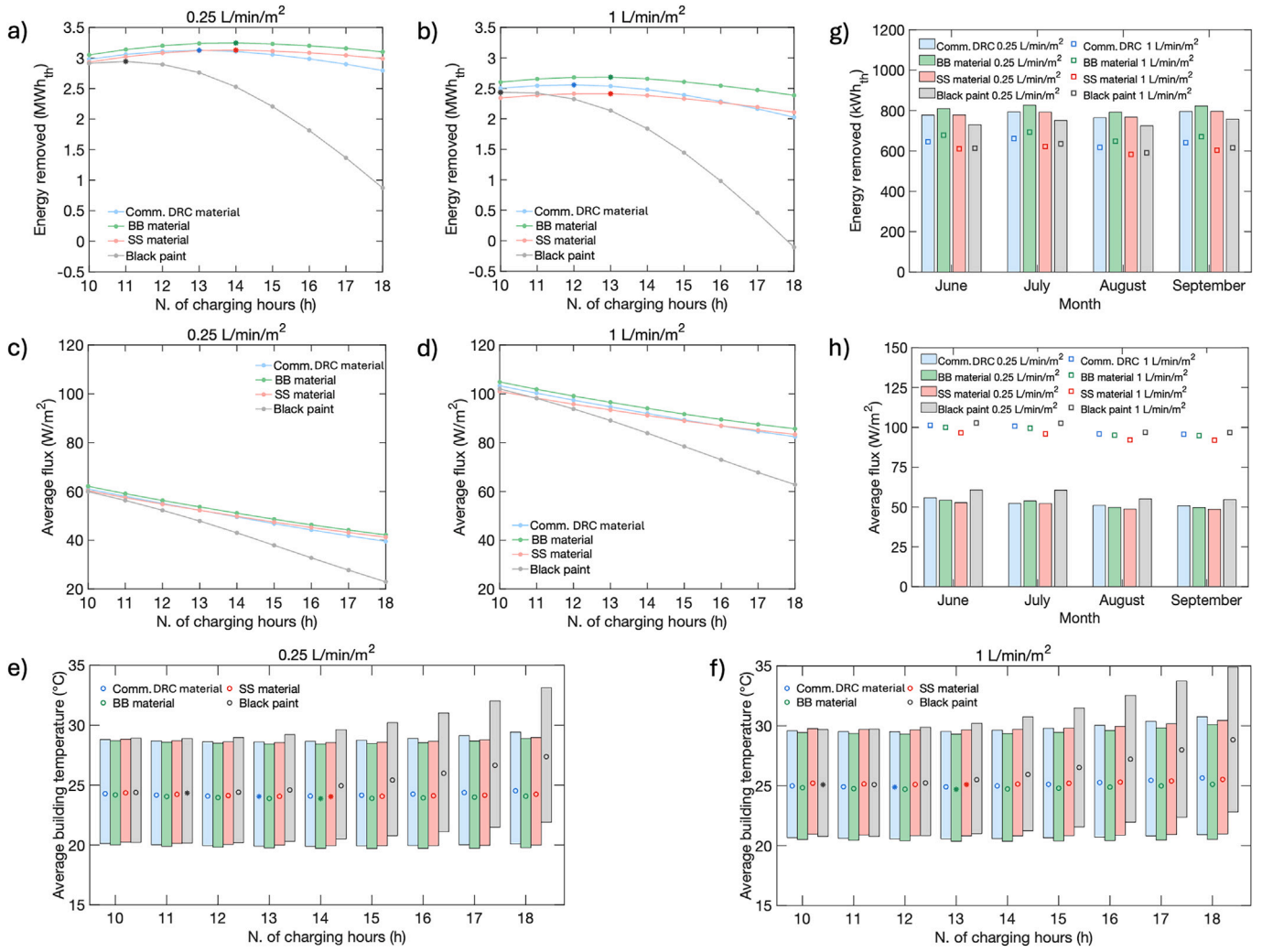

Fig. 4. Analysis of pumping hours in a single-family building in Madrid using a commercial DRC emitter, an ideal BB emitter, an ideal SS emitter, and conventional black paint. The number of SRs and RCMs are kept constant, respectively to 25 and 60. a–b) Energy removed by the RCMs operating at flow rates of 0.25 and 1 L min^{-1} m^{-2}, respectively. c–d) Average SR flux at flow rates of 0.25 and 1 L min^{-1} m^{-2}, respectively. e–f) Mean, maximum, and minimum indoor air temperatures with SR flow rates of 0.25 and 1 L min^{-1} m^{-2}, respectively. Mean values are indicated by the markers, while minimum and maximum temperatures define the extent of the bars. g-h) Monthly energy removed by RCMs and average flux, respectively, under optimal conditions (i.e., at the number of pumping hours that maximizes energy removal) for flow rates of 0.25 and 1 L min^{-1} m^{-2}. In panels a, b, e and f, the optimal number of pumping hours for each emitter type is marked with an asterisk.

to the significant heating of the black surface due to solar irradiance, which impairs its radiative cooling capability. Although DRC materials can ideally maintain sub-ambient temperatures even under intense solar radiation, their performance also deteriorates beyond 13–14 pumping hours, depending on the flow rate. During high-irradiance periods, in fact, the water inside the SRs may still be cooled, but not sufficiently to provide effective indoor cooling when circulated through the RCMs.

As shown in Fig. 4(c) and (d), higher flow rates generally result in increased cooling fluxes. This is due to the higher average temperature of the SRs, which enhances radiative emission in accordance with the Stefan-Boltzmann law. Conversely, lower flow rates promote greater subcooling of the thermal fluid. As long as the fluid remains colder than the building environment, higher subcooling enables greater thermal energy extraction. This trade-off explains why, despite higher cooling efficiency at 1 L min^{-1} m^{-2}, the total energy removed and, therefore, the actual cooling effect, is lower compared to a flow rate of 0.25 L min^{-1} m^{-2}. This highlights the critical importance of selecting an appropriate flow rate in systems without active cooling components such as heat pumps or HVAC units.

As illustrated in Figure S3, the optimal flow rate maximizing thermal energy removal is a function of the design of the hydronic system, specifically the surface areas of the SRs and RCMs. However, provided the SR surface is not significantly undersized, the optimal flow rate consistently lies within the range of 0.2–0.3 L min^{-1} m^{-2}. This finding is corroborated by extrapolations on the full-scale experimental setup, which also show an optimal flow rate within the same range across different meteorological conditions, and by other studies [66].

Fig. 4(e) and (f) present the average, minimum, and maximum indoor temperatures. The DRC materials yield lower average temperatures than the black emitter, with performance differences increasing at longer pumping durations. Lower flow rates (0.25 L min^{-1} m^{-2}) result in reduced mean, minimum, and maximum temperatures compared to 1 L min^{-1} m^{-2}. The minimum temperature is reached at 11 and 10 pumping hours for the black emitter, 13 and 12 for the commercial DRC, and 14 and 13 for the ideal BB and SS, respectively.

Fig. 4(g) and (h) show the monthly energy removed by the RCMs and the average SR flux, respectively, under optimal pumping durations (maximizing the energy removed by RCMs). DRC materials extend

the effective cooling window throughout the season. The ideal BB consistently outperforms the commercial DRC and ideal SS. Additionally, performance at 0.25 L min^{-1} m^{-2} is superior to 1 L min^{-1} m^{-2} across all months. The highest relative improvement over the nighttime emitter occurs in June (+6.5 % for the commercial DRC, +10.9 % for the ideal BB), and the lowest in September (+5.0 % and +8.6 %, respectively). Fig. 4(g) and (h) also demonstrate that, in hydronic cooling systems of this type, higher net cooling fluxes do not necessarily indicate a greater amount of energy removed from the indoor environment.

3.3. RCMs and SRs sizing

Having demonstrated the superior performance of the DRC-based hydronic cooling system compared to an equivalent configuration utilizing only nighttime radiative emitters, a sensitivity analysis is now required to determine the optimal sizing of the RCMs and SRs. Designing this system primarily involves determining the optimal surface areas for the SRs and RCMs. Ideally, both surfaces should be minimized while still ensuring continuous thermal comfort within the building.

3.3.1. Comfort index definition

To quantify thermal comfort, a metric called the comfort index (CI) is introduced. This indicator measures the fraction of time during which the average indoor air temperature of the building (T_b) remains within a predefined target range, delimited by a minimum and a maximum target temperature T^*_{min} and T^*_{max}. It is defined using the indicator function χ:

$$\chi(t) = \begin{cases} 1, & \text{if } T^*_{min} \le T_b(t) \le T^*_{max} \\ 0, & \text{otherwise} \end{cases} \tag{10}$$

The comfort index is then given by:

$$CI = \frac{1}{t_{tot}} \int_0^{t_{tot}} \chi(t) dt \tag{11}$$

where t_{tot} is the total simulation time.

Defining the comfort range for the building under analysis is a non-trivial task, as it does not fall strictly under the categories of either mechanically ventilated or naturally ventilated buildings. However, the DRC-based hydronic system more closely resembles a naturally ventilated configuration, as it lacks active components for air circulation, unlike mechanically ventilated systems. Moreover, while the DRC-hydronic system can be actively switched on or off, its performance cannot be precisely controlled via a setpoint, as it depends heavily on atmospheric conditions.

The ASHRAE-55 standard provides a method for defining comfort zones in buildings without mechanical ventilation [67,68]. Applying this method using the average ambient temperature for August, the hottest month in Madrid according to TMY data, and therefore selected for system sizing, yields a comfort range of 23.8 °C to 28.8 °C (see Supplementary Material, Section S6). To be conservative, the upper bound of the comfort range was reduced to T^*_{max} = 27 °C. The lower bound T^*_{min} was not imposed, to assess the natural cooling limits of the DRC system and also because the system can simply be switched off in case the indoor temperatures become excessively low.

3.3.2. Optimal SRs and RCMs sizes

To determine the optimal sizing of SRs and RCMs, extensive simulations were conducted for the month of August in Madrid. The simulations were performed using the commercial DRC emitter, a flow rate of 0.25 L min^{-1} m^{-2}, and 13 pumping hours, identified as optimal in previous analyses. Various combinations of RCM and SR areas were tested, and results are presented as color maps in Fig. 5, where the areas of SRs and RCMs are normalized relative to the floor area of the building.

Fig. 5(a) shows the variation of the comfort index. In general, there is no defined configuration maximizing CI; instead, CI increases monotonically with both SR and RCM surface areas. A comfort of about 100 % is achieved for a minimum SR coverage of 60 % (with 60 % RCM coverage). If the acceptable CI is set to 90 %, the configuration that minimizes simultaneously the total surface area of RCMs and SRs (i.e., the Pareto-optimal point) is found at approximately 47 % RCM and 53 % SR coverage. This corresponds to about 70 RCMs (56.7 m^2) and 28 SRs (63.6 m^2).

Fig. 5(b) presents the variation of average SR flux. The flux increases with RCM area and decreases with SR area. This inverse relationship with SR area arises because, at a fixed RCM size, increasing the SR area distributes the removed heat over a larger surface. As a result, the temperature of each SR decreases, leading to a reduction in radiative flux due to the lower surface temperature.

Fig. 5(c) and (d) illustrate the impact of the hydronic cooling system on the building. Specifically, panel c) presents the average reduction in indoor air temperature achieved in the building relative to the same building without the hydronic cooling system (i.e., the cooling effect). Panel d) displays the specific energy removed, defined as the daily thermal energy dissipated by the RCMs, normalized by the surface area of the SRs. The cooling effect increases with both SR and RCM area, similar to the trend observed in the comfort index. In contrast, the energy removed follows a trend similar to that of average SR flux: it increases with RCM area and decreases with SR area. This is because larger RCM coverage and smaller SR surfaces result in higher average SR temperatures and, consequently, higher radiative fluxes. The absolute energy removed, on the other hand, follows a different trend (shown in Figure S4a), analogous to that of the cooling effect.

Fig. 5(e) and (f) show the relative improvement in the comfort index for hydronic systems using a commercial DRC and an ideal BB emitter, respectively, compared to an identical system operating with a nighttime emitter (black emitter). In all cases, the systems operate at their respective optimal number of pumping hours. For both cases, the maximum improvement is observed at an SR coverage of approximately 30 % (corresponding to about 15 SRs), with gains of +8.7 % for the commercial DRC and +13.2 % for the ideal BB.

It is worth noting that varying the number of RCMs is equivalent to varying the total storage water volume of the system. Therefore, the results shown in Fig. 5 can also be interpreted in terms of storage water volume versus SR area, given that each RCM (with a bottom surface area of 0.81 m^2) contains approximately 50 L of stationary water.

3.4. Effect of plant configuration

3.4.1. Configurations analyzed

The analysis is further extended by evaluating the performance of the DRC-hydronic cooling system under three scenarios (external SRs, rooftop SRs and DRC-roof) and at two selected locations: Madrid and Rome.

The initial scenario, adopted in the preceding analysis, involves the installation of SRs on surfaces external to the building (Fig. 1(a)). In contrast, the second scenario considers the installation of SRs directly on the building rooftop (Fig. 1(b)). Installing SRs on the rooftop offers several advantages. First, it confines the spatial footprint of the plant to the footprint of the building itself. Second, it reduces the absorption of solar irradiance by the roof during daylight hours, particularly during periods of high irradiance when the cooling system is not operating, behaving as a fully passive DRC surface. Additionally, in urban environments, rooftop installation is likely to provide greater access to the sky dome and reduce the screening effect of airborne particulate matter [69]. At the same time, however, this configuration also brings some limitations. The available surface area is constrained by the roof dimensions, potentially reducing the number of SRs that can be installed. Furthermore, the rooftop may be subject to competition among other rooftop technologies, such as solar photovoltaic and solar thermal systems, and any proposed installation must comply with the structural capacity and constraints of the roof. Despite these limitations, the potential impact of rooftop SR installation is relevant and is therefore analyzed in this work.

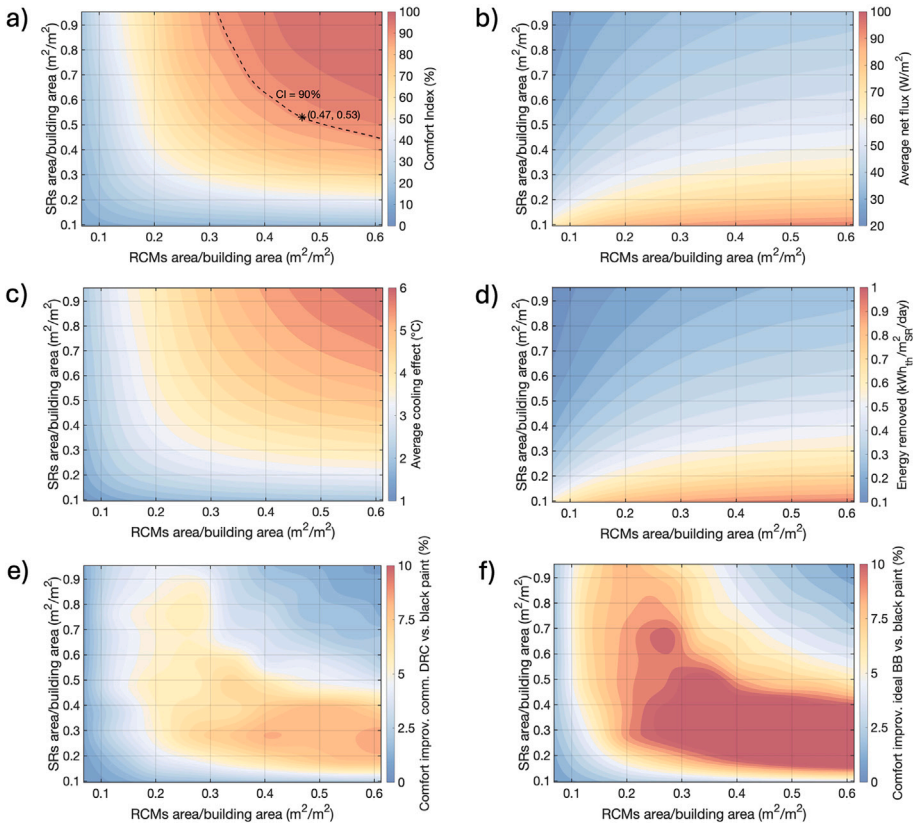

Fig. 5. SRs and RCMs sizing analysis for a single-family building in Madrid during August (TMY). a) Comfort index. b) Average SR flux. c) Average indoor temperature reduction compared to a passive building (no hydronic cooling). d) Specific thermal energy removed by RCMs. e) Comfort index improvement relative to a nighttime radiative cooling system. f) Comfort index improvement relative to a nighttime radiative cooling system, using the ideal BB material. All panels, except f), refer to the commercial DRC emitter.

In addition to the external and rooftop hydronic cooling system configurations, a third scenario is considered in which the building is equipped with a DRC-roof. In this case, no active components are employed, and the building roof is entirely covered with a passive DRC material, as illustrated in Fig. 1(c).

For all the configurations analyzed, the roof is assumed to be perfectly flat. To ensure consistency and comparability across different scenarios, the roof is considered to be entirely covered by the DRC technology, either in the form of SRs or as a continuous passive coating. According to the reference description of the two-story building, the total available roof area is 67.7 m^2, which, in the case of SR deployment, corresponds to approximately 29 SRs. External and rooftop SR configurations were tested using the same number of RCMs: 70 units (corresponding to a coverage of approximately 48 %).

3.4.2. Comparison across configurations

Fig. 6(a) and (b) present the average, maximum, and minimum indoor temperatures for the three analyzed configurations (external SRs, rooftop SRs, and DRC-roof) for the buildings located in Madrid and Rome, respectively. While the buildings in both locations share the same habitable surface area, they differ slightly in thermal insulation, as detailed in Tab. S1, in accordance with national standards. In both locations, the configurations employing SRs exhibit comparable performance, with the rooftop SRs demonstrating slightly lower indoor temperatures across the cooling season. Specifically, the average seasonal indoor temperatures achieved are 23.8 °C and 23.5 °C in Madrid, and 23.7 °C and 23.6 °C in Rome, for the external and rooftop SRs, respectively. In all cases, these values remain consistently below the adopted maximum thermal comfort threshold of 27 °C. In contrast, the passive DRC-roof configuration demonstrates limited cooling performance, with average seasonal temperatures exceeding the comfort limit: 28.1 °C in Madrid and 27.6 °C in Rome.

Fig. 6(c) and (d) show the seasonal comfort index for the three configurations, along with the relative improvement over a reference fully passive building with a conventional roof. Once again, the rooftop SR configuration slightly outperforms the external SRs. In Madrid, the seasonal CI values are 92.0 % and 96.4 % for external and rooftop SRs, respectively; in Rome, the values are 96.7 % and 97.4 %, respectively. The relative CI improvement with respect to the reference case is +64.0 % and +68.4 % in Madrid, and +59.1 % and +59.8 % in Rome, for external and rooftop SRs, respectively.

The consistently high seasonal CI values, always above 90 % and approaching 100 %, demonstrate the effectiveness of the DRC-based hydronic cooling system in delivering thermal comfort under the examined climatic conditions and building typologies. These results confirm that the surface area of SRs was appropriately sized to meet the thermal load requirements of both locations. In particular, limiting the extension of SRs to the roof area is sufficient to ensure suitable comfort levels.

On the other hand, the DRC-roof configuration alone fails to provide acceptable thermal comfort, with CI values of only 34.2 % in Madrid and 40.6 % in Rome. This poor performance can be attributed to the considerable roof insulation in both buildings; insulation negatively impacts fully passive radiative cooling by hindering heat transmission through the roof thickness [15]. While the DRC-roof is inadequate as a stand-alone cooling solution, it can contribute to significant reductions in electricity demand when integrated with active cooling systems [14–21]. As previously observed, the rooftop SRs configuration combines the active cooling effect of external SRs with the enhanced

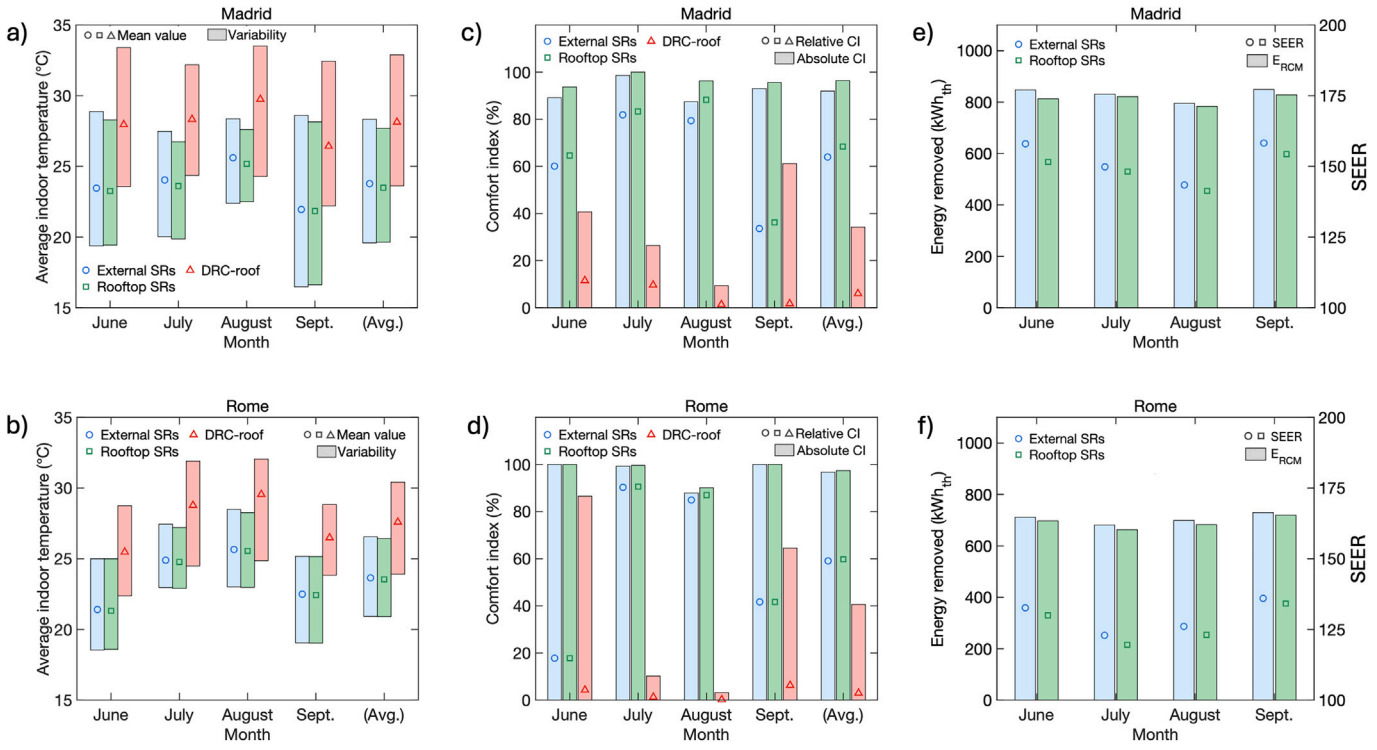

Fig. 6. Performance analysis for a single-family building in Madrid and Rome during the cooling season (TMY) under three scenarios: DRC-hydronic system with external SRs (blue), DRC-hydronic system with rooftop SRs (green), and a passive DRC roof (red). a–b) Average, maximum, and minimum indoor temperatures for Madrid and Rome, respectively. c–d) Comfort index (bars) and relative improvement (markers) with respect to a fully passive building with a conventional roof for Madrid and Rome, respectively. e–f) Total energy removed by the RCMs (bars) and system SEER (markers). In all simulations, the roof is assumed to be fully covered with commercial DRC material; for the external and rooftop SR configurations, this corresponds to 29 SRs. The DRC-hydronic system operates with the optimal number of daily pumping hours, at a flow rate of 0.25 L min^{-1} m^{-2}; it includes 70 RCMs.

solar reflectivity of a DRC-roof during daytime hours. However, the resulting comfort improvement is not a simple superposition of these two effects. In fact, the additional benefit of rooftop SRs over external SRs, in terms of comfort index, is relatively modest: +4.4 % in Madrid and +0.6 % in Rome. The primary reason for this limited improvement lies in the thermal insulation characteristics of the roof. Installing SRs directly on the roof introduces an additional insulating layer, mainly due to the water contained within the panels, which reduces the inward-to-outward heat flow, particularly during nighttime. This behavior is analogous to the reduced effectiveness of radiative cooling roofs when roof thermal insulation is increased. Therefore, the increased albedo effect introduced by rooftop SRs yields only a very limited impact on the energy balance of the building during the hot season and, by extension, also during the cold season. In line with the CI results, the rooftop and external SRs configurations exhibit very similar net cooling fluxes when sky access is equivalent. In non-ideal scenarios, however, the external SR configuration may experience reduced net fluxes due to limited sky access caused by the building itself.

3.4.3. Considerations on the energy efficiency of the system

To assess the overall energy performance of the hydronic cooling system through a single performance indicator, an approach analogous to that used for mechanical refrigeration systems can be adopted. Specifically, in the case of heat pumps in cooling mode, the Seasonal Energy Efficiency Ratio (SEER) is defined as the ratio between the useful thermal effect—namely, the energy extracted by the evaporator to provide cooling—and the electrical energy consumed by active components such as the compressor and fans. A similar concept can be introduced for the DRC-hydronic system, where the useful effect is represented by the thermal energy removed by the RCMs (E_{RCM}), and the energy input corresponds to the electricity consumed by the circulation pump ($E_{el,pump}$), which is the only active component of the system. Accordingly, an equivalent SEER for the hydronic system is defined as:

$$\mathrm{SEER} = \frac{E_{\mathrm{RCM}}}{E_{\mathrm{el,pump}}}. \tag{12}$$

The quantity E_{RCM} is determined through a thermal energy balance on the RCMs, while $E_{el,pump}$ is calculated based on the water flow rate, pressure losses in the circuit, pump efficiency and working time. Further details on the calculation methods for both terms are provided in the Supplementary Material, Section S4.

Fig. 6(e)–(f) present the monthly values of E_{RCM} and the corresponding SEER for Madrid and Rome, respectively. The resulting SEER values are proportional to the values of E_{RCM}, since the energy consumed by the pump is primarily determined by the total pumping time, which is roughly constant across all scenarios. Madrid achieves the highest SEER values: 152 for external SRs and 149 for rooftop SRs. In Rome, the values are slightly lower, at 129 and 127, respectively.

A first observation concerns the magnitude of these SEER values. For reference, the average SEER of conventional room air conditioners in the European building sector is approximately 5.4 [70]. This means that the DRC-based hydronic system can deliver a SEER up to 28 times higher than common AC systems in modern standard-insulated single family buildings. This remarkable performance is primarily attributed to the low electricity demand of the system, with the circulation pump being the only active component. These SEER values could be further improved by enhancing the thermal insulation of the water distribution pipelines. Another point of interest is the slightly lower SEER observed for rooftop SR configurations compared to external SRs. This difference arises because the rooftop DRC layer reduces solar heat gains, thereby

decreasing the overall cooling demand and, in turn, the energy removal by the RCMs.

Moreover, SEER can serve as a useful monthly performance metric for evaluating radiative cooling effectiveness. In both Rome and Madrid, the highest SEER values are recorded in June and September, months typically characterized by favorable conditions for radiative cooling [63]. By contrast, in July and August, radiative cooling is significantly hindered by high ambient temperatures and increased convective heat gains. However, it is important to clarify that, although the SEER has been defined in a manner similar to that of heat pumps, hydronic DRC-based cooling systems differ significantly from heat pumps. The latter are well-established technologies that enable precise indoor temperature control across all climates and, unlike DRC-based systems, are less heavily influenced by external weather conditions.

4. Discussion

In the previous analysis, the DRC-based hydronic cooling system has been demonstrated to be an effective, stand-alone and nearly passive solution for achieving adequate thermal comfort in single-family buildings in the temperate climates of Madrid and Rome. The system provides substantially higher comfort indices compared to a fully passive DRC-roof configuration and achieves significantly greater SEER values than conventional mechanical cooling systems. Nevertheless, the implementation of this technology may encounter certain limitations, the most relevant being its strong site-specificity. The performance of DRC-based hydronic systems depends significantly on the building typology, the density of the surrounding urban environment, and the climatic zone in which the system is deployed.

The required surface area of SRs increases with the cooling demand and, in some cases, may exceed the area available for a typical residential building. As previously discussed, one potential mitigation strategy involves relocating the SRs to the rooftop, thereby taking advantage of the additional albedo effect. However, rooftop areas may prove insufficient in locations with high cooling demands or in buildings with low roof-to-volume ratios. In general, this type of system is best suited for single-story buildings with large roof surfaces, such as warehouses, while it may be undersized for multi-story buildings. In the case of the two-story residential building considered in this study, the required SR surface to achieve acceptable comfort levels was approximately equal to the total roof area. Furthermore, rooftop SR installation may compete with other rooftop technologies, such as photovoltaic or solar thermal systems, thereby posing additional constraints.

To address these challenges, minimizing the surface area required for the SRs is of primary importance. A straightforward, yet effective, strategy involves improving the thermal insulation of the piping network, which is otherwise subject to considerable convective heat losses. Fig. 7(a) and (b) present the comfort index map and the indoor cooling effect, respectively, for varying numbers of SRs and RCMs in Madrid, under the assumption of a 90 % reduction in pipe thermal losses compared to the previous analyses. This reduction can be achieved by adopting approximately 35 mm of standard polyurethane insulation. As before, the Pareto-optimal configurations minimizing the combined surface areas of SRs and RCMs were identified. This improvement yields notable benefits: in Madrid, the required SR surface is reduced by approximately 9 % (equivalent to 4–5 fewer SRs).

Fig. 7(c)-(d) present the comfort index map and the indoor cooling effect, respectively, for Madrid under the combined effect of improved pipe insulation (90 % loss reduction), enhanced window shading and improved nighttime ventilation. In the base case, only the shading provided by window recesses was considered, assuming that solar light was free to illuminate the inside of the rooms. Here, an improved scenario assumes that 80 % of direct solar radiation is blocked throughout the entire season through the use of window sun shadings. Additionally, the building is assumed to be naturally ventilated, incorporating vents designed to enable wind-driven ventilation. This strategy is represented in the simulation by a constant nighttime (10:00 PM to 8:00 AM) air change rate of 5 air changes per hour (h^{-1}). Although actual ventilation rates in wind-driven systems vary with wind speed and direction [71], a constant rate was used here to evaluate the potential benefits of effective nighttime ventilation. These improvements, addressing both the hydronic system and building physics, result in a drastically reduced coverage requirement: 17 % for RCMs and 19 % for SRs with respect to the base scenario. This demonstrates that the DRC-based hydronic system can be particularly effective in modern standard-insulated and naturally ventilated residential buildings equipped with solar shadings.

Since the performance of the DRC-driven hydronic cooling system relies on the thermal exchange between the SRs and the sky dome, the deployment of the technology is strongly hindered in locations with

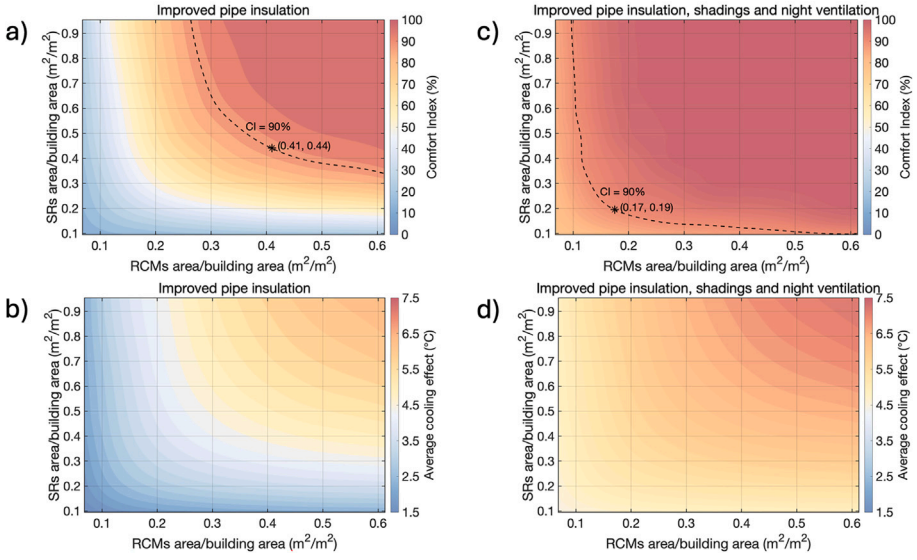

Fig. 7. SRs and RCMs sizing analysis for a single-family building during August (TMY) in Madrid, using the commercial DRC emitter, a flow rate of 0.25 L min^{-1} m^{-2} and the optimal number of pumping hours. a) Comfort index with enhanced pipe insulation. b) Average indoor temperature reduction compared to a passive building (no hydronic cooling and conventional roof) with enhanced pipe insulation. c) Comfort index with enhanced pipe insulation, sun shadings and nighttime ventilation. d) Average indoor temperature reduction compared to a passive building with enhanced pipe insulation, sun shadings and nighttime ventilation.

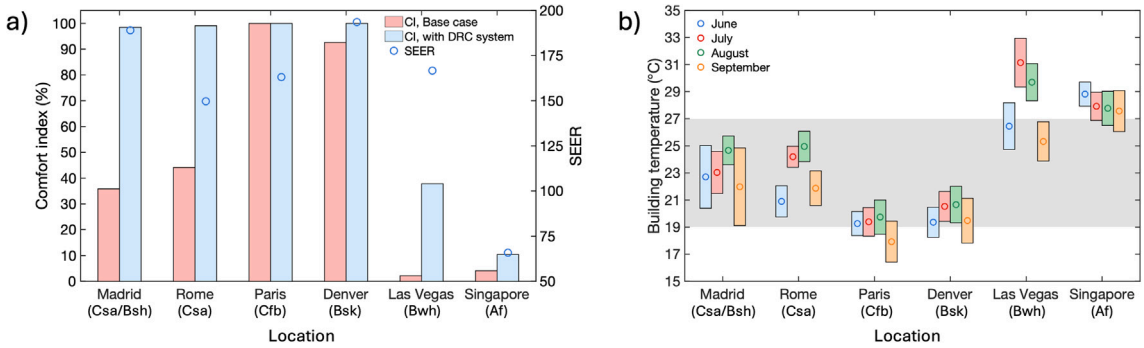

Fig. 8. Effect of location on: a) Comfort Index in a fully passive building (red bars) and in a building equipped with the DRC-based hydronic cooling system (blue bars), with SEER indicated by markers; b) Indoor building temperatures (where markers indicate average values and bars represent variability). The analysis considers a single-family building (same for all locations) during the June-September season (TMY), with full roof coverage of SRs, 70 RCMs, a flow rate of 0.25 L min^{-1} m^{-2}, and enhanced pipe insulation.

limited sky access or in climates characterized by warm and cloudy skies. In dense urban environments, sky access—quantified by the sky view factor—can be substantially reduced, with average values falling as low as 50–60 % [72]. In such contexts, the thermal energy balance of the SRs must be modified to account for infrared emission from neighboring obstacles, such as adjacent buildings, and their shading effect [73]. Estimates from the present work (see Supplementary Material, Section S8 and Figure S7(a)) indicate that a reduction of the sky view factor to approximately 80 %, a reasonable value for rooftop installations, may result in significant SEER reductions.

While the DRC-based hydronic cooling system has been demonstrated as a stand-alone solution for building cooling in the temperate climates of Madrid and Rome, integration with conventional cooling systems, such as HPs or HVAC units, may be required to maintain adequate comfort in climates with extremely high cooling demand or conditions unfavorable for radiative cooling. To assess this, the same building equipped with the DRC-based hydronic system was evaluated in multiple locations worldwide, representing different climate conditions (according to Köppen-Geiger classification). For comparability, a consistent comfort zone was applied across all locations (indoor temperature considered comfortable below 27 °C), and the hydronic system was switched off whenever the temperature fell below 19 °C. Furthermore, a new dynamic feedback control strategy was adopted to replace the fixed-schedule approach, as the latter could not accommodate the strong variations in daylight hours and meteorological conditions across different locations. The new strategy activates the circulation pump only when the RCMs–SRs average temperature difference exceeds 0.5 °C, ensuring operation only during periods favorable for radiative cooling (see Supplementary Material, Section S10 for details).

Fig. 8(a) presents the results of this analysis in terms of CI and SEER, while Fig. 8(b) presents them in terms of indoor temperature. The previously analyzed locations of Madrid (Csa/BSh) and Rome (Csa) confirm that the adoption of a stand-alone DRC-based hydronic system is viable in temperate climates, achieving high absolute CI values (~99 %) and significant CI improvements compared to the base case. Additionally, owing to the improved control strategy, the SEER increases, reaching values up to 35 times higher than those of conventional AC systems in the Madrid case study and 28 times in Rome. Cooler summer climates, such as Paris (France, Cfb type) and warm dry summer climates, such as Denver (USA, BSk type), exhibit high CI values; however, the relative improvement compared to the base case is limited. In contrast, very hot climates—arid, as in Las Vegas (USA, BWh type), and tropical humid, as in Singapore (Af type)—show insufficient CI values and only moderate improvements relative to the base case. These results suggest that in such climates, the DRC-based hydronic implementation may be insufficient, and configurations including a conventional AC backup system should be preferred. Alternatively, other DRC-integrated AC configurations could be deployed [31,37,40] to enhance comfort under extreme conditions.

While the technical viability of a stand-alone DRC system has been widely demonstrated under the climatic conditions of Madrid and Rome, its economic viability should also be explored. According to a preliminary economic analysis (see Supplementary Material, Section S11 for details) performed for the Madrid and Rome case studies, the capital expenditure of the proposed DRC system is significantly higher than that of conventional residential heat pumps, primarily due to the high costs of the SRs and RCMs. However, the operational expenditure is negligible—approximately 25–55 times lower than that of heat pumps, depending on the efficiency of the latter. In addition, cooling season carbon dioxide emissions can be reduced by approximately 80–150 kg of CO_2 compared to conventional cooling systems. These results suggest that the very low operating costs and emissions may partially offset the higher initial investment, especially in the presence of green incentives. Moreover, the potential to extend the DRC-based cooling system to year-round operation using switchable radiative-cooling/solar-heating materials [74,75] could further enhance its long-term economic viability.

Another potential limitation of the DRC-based hydronic cooling system concerns condensation on the hydronic surfaces [47] and on the SRs. In the case of SRs, the presence of water can degrade the optical performance of the DRC material, thereby reducing its radiative performance [76,77]. Under conditions of high relative humidity, the surface temperature of DRC elements may fall below the ambient dew point, leading to condensation of atmospheric moisture. However, for the hydronic DRC-based system analyzed in this study, the impact of condensation remains limited (see Supplementary Material, Section S7 and Figure S6). This is primarily due to the moderate cooling of SRs, which typically operate only a few degrees below ambient temperature, and avoid the deeper subcooling associated with fully passive DRC systems. The seasonal occurrence of condensation is below 0.03 % of the total operational time in Madrid, and approximately 0.3 % in Rome.

In order to favor condensation removal from the surface of SRs, in real applications they should be mounted with a slight inclination, enabling gravity-assisted water drainage. Furthermore, a northward tilt may also be beneficial for radiative cooling, as it reduces the overall solar exposure [78].

Finally, natural aging and soiling, affecting the optical properties of DRC materials, may reduce the cooling efficiency of the DRC-based hydronic system [79,80]. Among natural aging phenomena, one of the most impactful is ultraviolet-induced degradation, which may compromise the solar reflectivity of DRC surfaces over time [81]. Nevertheless, the DRC-based hydronic system presented in this work is only marginally affected by reductions in solar reflectivity (see Figure S7(b)), since its operation occurs primarily at night and during periods of low to moderate solar irradiance.

5. Conclusion

In this work, a DRC-based hydronic cooling system was presented, modeled, and validated using experimental data from a full-scale demonstrator. The system was shown, through dynamic simulations, to achieve full thermal comfort in a real-scale single-family residential building under TMY conditions for the cooling season in Madrid (Spain) and Rome (Italy). The validated model was further used to explore the influence of various design parameters, including the number of SRs and RCMs, water flow rate and pumping hours. The main findings of this study can be summarized as follows:

(1) The DRC-based hydronic system was compared against a system employing a conventional nighttime emitter (black paint). Under the tested flow conditions, the use of DRC emitters extended the operating window of the system by 2–3 hours.
(2) A parametric study of different combinations of RCM and SR surface areas during the cooling season in Madrid showed that a comfort index greater than 90 % can be achieved with an RCM/SR coverage of 47 %/53 %. By improving the DRC system design and control strategy, comfort index values around 99 % are attainable.
(3) The performance of a hydronic system with external SRs was compared to a rooftop SRs configuration, which benefits from the increased roof albedo. Both configurations successfully achieved thermal comfort under the climates of Madrid and Rome, with the rooftop SRs offering slightly improved performance. In contrast, a fully passive DRC roof failed to maintain acceptable indoor comfort levels.
(4) The seasonal energy efficiency ratio of the DRC-based hydronic system reached values approximately 35 times higher than those typically reported for conventional mechanical air conditioning systems in the case of Madrid, although conventional systems can maintain a more precise comfort range and offer better controllability.
(5) Enhancing the thermal insulation of the distribution piping, incorporating effective solar shading for windows and improving the nighttime ventilation strategy significantly reduced the required surface coverage of both RCMs and SRs. In Madrid, a combined coverage as low as 17 % (RCMs) and 19 % (SRs) was sufficient to achieve thermal comfort.

These findings underscore the potential of DRC materials in achieving energy-efficient and almost completely passive cooling systems for buildings. Such technologies represent a promising avenue for sustainable building design, particularly in mitigating the urban heat island effect and city-wide overheating. However, several barriers must be addressed for large-scale adoption. These include the relatively high initial cost of DRC materials, limited applicability in high-rise buildings and dense urban environments, and performance degradation due to condensation, natural aging, and soiling. Ongoing research and innovation are critical to overcoming these challenges and facilitating the integration of radiative cooling into mainstream building systems. Future studies should also prioritize the development of advanced flow rate control strategies to optimize performance under changing weather conditions, integration of thermal water storage to decouple the hydronic and DRC circuits for improved system flexibility, the use of switchable radiative-cooling/solar-heating materials for year-round operation, and the investigation of the screening effects caused by ceiling-mounted radiant capacitive modules.

CRediT authorship contribution statement

Davide Forte: Writing – original draft, Visualization, Software, Methodology, Investigation, Formal analysis, Data curation. **Eduardo González-Cruz:** Writing – review & editing, Validation, Supervision, Resources, Formal analysis, Data curation, Conceptualization. **Lorenzo Pattelli:** Writing – review & editing, Validation, Supervision, Project administration, Methodology, Funding acquisition. **Claudio Belotti:** Writing – review & editing, Methodology, Formal analysis, Data curation. **Gloria Perez:** Writing – review & editing, Validation, Resources, Project administration, Funding acquisition. **Pietro Asinari:** Writing – review & editing, Validation, Supervision, Project administration. **Matteo Fasano:** Writing – review & editing, Validation, Supervision, Project administration, Methodology, Conceptualization.

Declaration of competing interest

The authors declare that they have no known competing financial interests or personal relationships that could have appeared to influence the work reported in this paper.

Acknowledgments

The authors acknowledge the project PaRaMetriC (21GRD03, Metrological framework for passive radiative cooling technologies), which received funding from the European Partnership on Metrology, co-financed by the European Union's Horizon Europe Research and Innovation Programme and the Participating States.

Appendix A. Supplementary data

Supplementary data for this article can be found online at doi:10.1016/j.apenergy.2025.127260.

Data availability

The complete dataset of model results will be made available on request. The atmospheric data used are available open access in the associated Zenodo repository at https://doi.org/10.5281/zenodo.17227622

References

[1] International Energy Agency. The future of cooling. Opportunities for energy-efficient air conditioning. Paris: IEA; 2018. https://www.iea.org/reports/the-future-of-cooling. Licence: CC BY 4.0.
[2] International Energy Agency. Space cooling; 2023. https://www.iea.org/energy-system/buildings/space-cooling [Retrieved Jul 7, 2025].
[3] Woods J, James N, Kozubal E, Bonnema E, Brief K, Voeller L, Rivest J. Humidity's impact on greenhouse gas emissions from air conditioning. Joule 2022;6(4):726–41.
[4] Augello L, Naik A, Morciano M, Brugård J, Fasano M. Acausal equation-based and object-oriented modeling of heating systems: the college thermal library. Case Stud Therm Eng 2023;45(102894).
[5] International Energy Agency. Energy efficiency 2022, 2022.
[6] Alberghini M, Morciano M, Fasano M, Bertiglia F, Fernicola V, Asinari P, Chiavazzo E. Multistage and passive cooling process driven by salinity difference. Science Adv 2020;6(11):5015.
[7] Tabasian AN, Saija A, Morciano M, Fasano M, Tiraferri A, Chiavazzo E. Performance analysis of a scalable solar-assisted pilot scale adsorption desalination and cooling system. Energy Convers Manag 2025;343(120190).
[8] Pirvaram A, Talebzadeh N, Leung SN, O'Brien PG. Radiative cooling for buildings: a review of techno-enviro-economics and life-cycle assessment methods. Renew Sustain Energy Rev 2022;162(112415).
[9] Chen J, Lin L. Development of radiative cooling and its integration with buildings: a comprehensive review. Solar Energy 2020;212:125–51.
[10] Zhao B, Mingke H, Xianze A, Chen N, Pei G. Radiative cooling: a review of fundamentals, materials, applications, and prospects. Appl Energy 2019;236:489–513.
[11] Raman AP, Anoma MA, Zhu L, Rephaeli E, Fan S. Passive radiative cooling below ambient air temperature under direct sunlight. Nature 2014;515(7528):540–4.
[12] Carlosena L, Ruiz-Pardo Á, Feng J, Irulegi O, Hernández-Minguillón RJ, Santamouris M. On the energy potential of daytime radiative cooling for urban heat island mitigation. Sol Energy 2020;208:430–44.
[13] Li Z, Chen J, Wang C, Wang W, Yang F, Chen X, Zhang R, Pan A, Tsz Chung H, Lin K, et al. Enhancing sustainable urban environments in China: daytime radiative cooling for building energy efficiency and heat island mitigation. Appl Energy 2025;393(126138).
[14] Fan B, Yan D, Tan G, Sun H, Jingjing A. Systematically incorporating spectrum-selective radiative cooling into building performance simulation: numerical integration method and experimental validation. Appl Energy 2022;312(118733).
[15] Chen J, Lin L. Comprehensive evaluation of thermal and energy performance of radiative roof cooling in buildings. J Build Eng 2021;33(101631).
[16] Feng J, Saliari M, Gao K, Santamouris M. On the cooling energy conservation potential of super cool roofs. Energy and Build 2022;264(112076).
[17] Baniassadi A, Sailor DJ, Ban-Weiss GA. Potential energy and climate benefits of super-cool materials as a rooftop strategy. Urban Climate 2019;29(100495).

[18] Wang N, Yinyan L, Zhao D, Zhao W, Jingtao X, Yang R. Performance evaluation of radiative cooling for commercial-scale warehouse. Mater Today Energy 2022;24(100927).
[19] Xinxian Y, Chen C. Coupling spectral-dependent radiative cooling with building energy simulation. Build Environ 2021;197(107841).
[20] Chen J, Lin L, Gong Q, Lau WY, Cheung KH. Techno-economic and environmental performance assessment of radiative sky cooling-based super-cool roof applications in China. Energy Convers Manag 2021;245(114621).
[21] Chen J, Lin L, Gong Q. Techno-economic and environmental evaluation on radiative sky cooling-based novel passive envelope strategies to achieve building sustainability and carbon neutrality. Appl Energy 2023;349(121679).
[22] Yuan J, Yin H, Yuan D, Yang Y, Shaoyu X. On daytime radiative cooling using spectrally selective metamaterial based building envelopes. Energy 2022;242(122779).
[23] Xuan Q, Lao J, Zhao B, Guiqiang L, Pei G, Niu J, Dai J-G. Experimental and numerical investigation on energy-saving performance of radiative cooling coating for metal container office. Energy and Build 2024;310(114084).
[24] Zhang Y, Yang Z, Zhang Z, Cai Y, Sun Z, Zhang H, Yanwen L, Liu L, Zhang W, Xue X, et al. Sub-ambient cooling effect and net energy efficiency of a super-amphiphobic self-cleaning passive sub-ambient daytime radiative cooling coating applied to various buildings. Energy and Build 2023;284(112702).
[25] Wang S, Yang L, Liu Y, Pang J, Yang L, Dou M. Full-scale experimental study of the surface cooling effect of prefabricated buildings utilizing passive radiative cooling under real operating conditions. Energy 2025:136472.
[26] Wang T, Xuan Q, Dong Y, Lei D, Dai J-G. Bilayer fluorescent colored radiative cooling coatings for building energy saving. Energy 2025:137292.
[27] Cheng Z, Han H, Wang F, Yan Y, Shi X, Liang H, Zhang X, Shuai Y. Efficient radiative cooling coating with biomimetic human skin wrinkle structure. Nano Energy 2021;89(106377).
[28] Liu R, Xia K, Tao Y, Gao F, Zhang Q, Zhu L, Zhizhen Y, Yang S, Yaoguang M, Jianguo L. Multifunctional smart fabrics with integration of self-cleaning, energy harvesting, and thermal management properties. ACS Nano 2024;18(45):31085–97.
[29] Tao Y, Liu R, Yang Z, Yang S, Zhizhen Y, Jianguo L. Color design for daytime radiative cooling: fundamentals and approaches. Appl Energy 2025;377(124436).
[30] Jia L, Lin L, Gong Q, Jiao K. Analytical and experimental analyses on cooling performances of radiative Skycool radiators with various interior flowing channels. Energy 2024;295(130907).
[31] Goldstein EA, Raman AP, Fan S. Sub-ambient non-evaporative fluid cooling with the sky. Nature Energy 2017;2(9):1–7.
[32] Zhao D, Aili A, Zhai Y, Lu J, Kidd D, Tan G, Yin X, Yang R. Subambient cooling of water: toward real-world applications of daytime radiative cooling. joule 2019;3:111–23.
[33] Aili A, Zhao D, Jiatao L, Zhai Y, Yin X, Tan G, Yang R. A kW-scale, 24-hour continuously operational, radiative sky cooling system: experimental demonstration and predictive modeling. Energy Convers Manag 2019;186:586–96.
[34] Peoples J, Hung Y-W, Xiangyu L, Gallagher D, Fruehe N, Pottschmidt M, Breseman C, Adams C, Yuksel A, Braun J, et al. Concentrated radiative cooling. Appl Energy 2022;310(118368).
[35] Fiorentini M, Cooper P, Zhenjun M. Development and optimization of an innovative HVAC system with integrated pvt and PCM thermal storage for a net-zero energy retrofitted house. Energy and Build 2015;94:21–32.
[36] Vilà R, Medrano M, Castell A. Numerical analysis of the combination of radiative collectors and emitters to improve the performance of water-water compression heat pumps under different climates. Energy 2023;266(126445).
[37] Forte D, Belotti C, Pattelli L, Morciano M, Chiavazzo E, Asinari P, Fasano M. Modeling of daytime radiative cooling enhanced vapor-compression refrigeration systems. Energy 2025;340(139101).
[38] Zhang K, Zhao D, Yin X, Yang R, Tan G. Energy saving and economic analysis of a new hybrid radiative cooling system for single-family houses in the USA. Appl Energy 2018;224:371–81.
[39] Jia L, Cui P, Lin L, Chen J, Cao Z. Parametric analysis and potential evaluation of an all-day radiative sky cooling radiator-assisted ground source heat pump system. Appl Therm Eng 2024;240(122285).
[40] Aili A, Long W, Cao Z, Wen Y. Radiative free cooling for energy and water saving in data centers. Appl Energy 2024;359(122672).
[41] Ribezzo A, Bergamasco L, Morciano M, Fasano M, Mongibello L, Chiavazzo E. Experimental analysis of carbon-based phase change materials composites for a fast numerical design of cold energy storage systems. Appl Therm Eng 2023;231(120907).
[42] González-Cruz EM, Krüger EL. Experimental study on a low energy radiant-capacitive heating and cooling system. Energy Build 2022;255(111674).
[43] Mokhtari R, Ghasempour R. Feasibility study of integration of radiative cooling and hydronic radiant system for free cooling of single-family houses. Appl Therm Eng 2023;220(119629).
[44] Yuan J, Yin H, Cao P, Yuan D, Shaoyu X. Daytime radiative cooling of enclosed water using spectral selective metamaterial based cooling surfaces. Energy Sustain Dev 2020;57:22–31.
[45] Mokhtari R, Ulpiani G, Ghasempour R. The cooling station: combining hydronic radiant cooling and daytime radiative cooling for urban shelters. Appl Therm Eng 2022;211(118493).
[46] Abraham DE, Yang R, Mandal J, Yore M, Xin Huang VKT, Wells W, Schwarz K, Eisenman DP, Raman AP. Efficient outdoor thermal comfort via radiant cooling and infrared-reflective walls. Nat Sustain 2025:1–9.
[47] Teitelbaum E, Chen KW, Aviv D, Bradford K, Ruefenacht L, Sheppard D, Teitelbaum M, Meggers F, Pantelic J, Rysanek A. Membrane-assisted radiant cooling for expanding thermal comfort zones globally without air conditioning. In: Proceedings of the National Academy of Sciences, 117. 2020. p. 21162–9(35).
[48] Chen KW, Teitelbaum E, Meggers F, Pantelic J, Rysanek A. Exploring membrane-assisted radiant cooling for designing comfortable naturally ventilated spaces in the tropics. Build Res Inf 2021;49(5):483–95.
[49] González-Cruz E, Pérez G, Borja F, Alonso C, Martin-Consuegra F, Krüger E, Gutierrez A, Arranz B. Full-scale facility for the assessment of night and daytime passive radiative cooling. In: Proceedings of 2024 CATE conference; [20–22 Nov 2024]; Seville, Spain; Nov 2024. p. 179.
[50] Adibekyan A, Schumacher J, Pattelli L, Jochen Manara SM, Bazkir, Carlo Cucchi CS, Pérez G, Campos J, et al. Emissivity and reflectivity measurements for passive radiative cooling technologies. Int J Thermophys 2025;46(5):1–16.
[51] National Renewable Energy Laboratory. Reference Air Mass 1.5 spectra; 2023. Retrieved. https://www.nrel.gov/grid/solar-resource/spectra-am1.5.html [Nov 5, 2023].
[52] Das AK, Iqbal M. A simplified technique to compute spectral atmospheric radiation. Solar Energy 1987;39(2):143–55.
[53] The MathWorks Inc. Simscape (version 24.1). Available at: 2022. https://www.mathworks.com.
[54] Loga T, Stein B, Diefenbach N. Tabula building typologies in 20 European countries—making energy-related features of residential building stocks comparable. Energy and Build 2016;132:4–12.
[55] Ministerio de la vivienda. Código técnico de LA edificación. Real Decreto 2006;314.
[56] Prada A, Baratieri M, Baggio P, Romagnoni P, Gasparella A, et al. Caratteristiche dinamiche dei componenti edilizi: metodi semplificati (UNI EN ISO 13786), modellazione dettagliata e dati sperimentali. Certificazione energetica: normative e modelli di calcolo per il sistema edificio-impianto posti a confronto; AICARR; 2008. 371–82.
[57] Iacono MJ, Delamere JS, Mlawer EJ, Shephard MW, Clough SA, Collins WD. Radiative forcing by long-lived greenhouse gases: calculations with the AER radiative transfer models. J Geophys Res Atmos 2008;113(D13).
[58] Atmospheric and Environmental Research Inc. Longwave rapid radiative transfer model (RRTM_LW). https://github.com/AER-RC/RRTM_LW.
[59] European Commission, Joint Research Centre. PVGIS: photovoltaic geographical information system; 2025. Access:. https://re.jrc.ec.europa.eu/pvg_tools/it/#TMY [2025 Jun 20].
[60] ISO 15927-4:2005—hygrothermal performance of buildings—calculation and presentation of climatic data—part 4: hourly data for assessing the annual energy use for heating and cooling. 2005.
[61] Hersbach H, Bell B, Berrisford P, Biavati G, Horányi A, Muñoz Sabater J, Nicolas J, Peubey C, Radu R, Rozum I, et al. ERA5 hourly data on single levels from 1940 to present, Copernicus Climate Change Service (C3S) climate data store (CDS). 2023. Accessed on May 23, 2025]. https://doi.org/10.24381/cds.adbb2d47
[62] Belotti C, Hameury J, Pattelli L. Atmospheric downward longwave irradiance (flux) calculated using PASTICHE (the PaRaMetriC atmospheric spectral tool for irradiance calculation using hourly ERA5 data). 2025 [Sep 2025].
[63] Yang Y, Zhang G, Rong L. Cooling energy savings from passive daytime radiative cooling in Europe: a comparative analysis with and without population weighting from open-source data, with additional comparisons to Chinese cities. Energy Convers Manag 2024;314(118616).
[64] Kottek M, Grieser J, Beck C, Rudolf B, Rubel F. World map of the Köppen-Geiger Climate classification updated. 2006.
[65] Yue H, Yue L, Gao S, Luo X, Sun L, Feng C. How to rapidly and accurately evaluate the cooling performance of radiative cooling materials? Renew Energy 2024;236(121503).
[66] Aketouane Z, Bruneau D, Sempey A, Bouzouidja R, Lagiere P, Raji S, Roger P. Development of a night-time radiative sky cooling production & storage system: a proposal for a robust sizing and potential estimation methodology. Appl Therm Eng 2022;211(118378).
[67] ASHRAE. ANSI/ASHRAE standard 55-2017: thermal environmental conditions for human occupancy. Atlanta: ASHRAE; 2017.
[68] Kazanci OB, Coakley D, Olesen BW. A review of adaptive thermal comfort implementation in international thermal comfort standards. In: 2019 ASHRAE annual conference; 2019.
[69] Wang X, Chen X, Bojun M, Zhou Z, Peng C. Observed vertical dispersion patterns of particulate matter in urban street canyons and dominant influencing factors. Forests 2024;15(8):1319.
[70] European Commission. Air conditioners and comfort fans. https://perma.cc/J5BT-ZXQN.
[71] Horan JM, Finn DP. Sensitivity of air change rates in a naturally ventilated atrium space subject to variations in external wind speed and direction. Energy and Build 2008;40(8):1577–85.
[72] Middel A, Lukasczyk J, Maciejewski R, Demuzere M, Roth M. Sky view factor footprints for urban climate modeling. Urban Clim 2018;25:120–34.
[73] Tang H, Chai X, Jing W, Yemao L, Chunying L. Assessment of photovoltaic power generation and radiative cooling potentials in old residential districts: a case study of Shenzhen. Energy and Build 2024;319(114493).
[74] Xiuqiang L, Sun B, Sui C, Nandi A, Fang H, Peng Y, Tan G, Hsu P-C. Integration of daytime radiative cooling and solar heating for year-round energy saving in buildings. Nat Commun 2020;11(1):6101.
[75] Liu J, Zhou Z, Zhang D, Jiao S, Zhang J, Gao F, Ling J, Feng W, Zuo J. Research on the performance of radiative cooling and solar heating coupling module to direct control indoor temperature. Energy Convers Manag 2020;205(112395).

[76] Simsek E, Mandal J, Raman AP, Pilon L. Dropwise condensation reduces selectivity of sky-facing radiative cooling surfaces. Int J Heat Mass Transf 2022;198(123399).
[77] Lavielle N, Othman AM, Hervé A, Hamaoui G, Fei J, Tan JY, Marty F, Hong L, Mongruel A, Beysens D, et al. Infrared spectral emissivity dynamics of surfaces under water condensation. Adv Funct Mater 2024;34(29):2403316.
[78] Zhao B, Xianze A, Chen N, Xuan Q, Mingke H, Pei G. General strategy of passive sub-ambient daytime radiative cooling. Sol Energy Mater Sol Cells 2019;199:108–13.
[79] Fan F, Qihao X, Zhao D. Heat transfer properties of dusty radiative cooling surface: modeling and experimental studies. Int J Heat Mass Transf 2023;214(124465).
[80] Yue H, Biao L, Fang J, Lei Y, Gao S, Feng C. Radiative cooling for long-term building energy efficiency: an experimental comparison of seven coatings. Natl Sci Open 2024;3(3):20230065.
[81] Song J, Shen Q, Shao H, Deng X. Anti-environmental aging passive daytime radiative cooling. Adv Sci 2024;11(10):2305664.